



HAL
open science

Numerical demonstration of surface lattice resonance excitation in integrated localized surface plasmon waveguides

Giovanni Magno, Benjamin Leroy, David Barat, Laetitia Pradere, Beatrice Dagens

► **To cite this version:**

Giovanni Magno, Benjamin Leroy, David Barat, Laetitia Pradere, Beatrice Dagens. Numerical demonstration of surface lattice resonance excitation in integrated localized surface plasmon waveguides. *Optics Express*, 2022, 30 (4), pp.5835. 10.1364/OE.449832. hal-03752295

HAL Id: hal-03752295

<https://hal.science/hal-03752295v1>

Submitted on 16 Aug 2022

HAL is a multi-disciplinary open access archive for the deposit and dissemination of scientific research documents, whether they are published or not. The documents may come from teaching and research institutions in France or abroad, or from public or private research centers.

L'archive ouverte pluridisciplinaire **HAL**, est destinée au dépôt et à la diffusion de documents scientifiques de niveau recherche, publiés ou non, émanant des établissements d'enseignement et de recherche français ou étrangers, des laboratoires publics ou privés.



Numerical demonstration of surface lattice resonance excitation in integrated localized surface plasmon waveguides

GIOVANNI MAGNO,^{1,2,4}  BENJAMIN LEROY,¹ DAVID BARAT,³
LAETITIA PRADERE,³ AND BEATRICE DAGENS^{1,5} 

¹Université Paris-Saclay, CNRS, Centre de Nanosciences et de Nanotechnologies, 91120, Palaiseau, France

²Department of Electrical and Information Engineering, Polytechnic University of Bari, Via Orabona, 4, 70125, Bari, Italy

³Groupe Stellantis, Direction Recherche et Ingénierie avancée, Centre technique de Velizy, route de Gisy, 78140 Velizy-Villacoublay, France

⁴giovanni.magno@poliba.it

⁵beatrice.dagens@c2n.upsaclay.fr

Abstract: We numerically show that surface lattice resonances (SLR) in periodic localized surface plasmon (LSP) waveguides integrated on a dielectric waveguide can be excited via in-phase evanescent coupling, by incident propagation vector outside the light cone and without any constraint on the structural symmetry. FDTD simulations show that the coupling between wideband LSP resonances and narrowband SLR results in a Fano-like resonance, showing few nanometers large sharp spectral features that may be exploited for achieving new functions for integrated optics and sensing.

© 2022 Optica Publishing Group under the terms of the [Optica Open Access Publishing Agreement](#)

1. Introduction

Localized surface plasmons polaritons (LSP) in noble metal nanoparticles (MNP) induce specific optical properties, such as extinction, absorption, and scattering of the light [1,2], that are affected by their size, shape, and environment. In 1D or 2D MNP lattice arrangement with a period near the wavelength, incident light extinction anomalies have been observed. These anomalies give rise to a very narrow lineshape above the LSP resonance wavelength. They have been identified as surface lattice resonances (SLR) - or lattice surface mode - by several groups [3–6]. From a physical point of view, the mechanism underlining the SLR involves grazing diffraction modes that in-phase interact with localized surface plasmonic resonances. From an analytical point of view, SLRs appear under conditions that vanish the imaginary part of each particle polarisability denominator [3,7,8]. These conditions require retardation effects in MNPs plasmonic resonance occurring for i) sufficiently large MNPs, ii) a lattice period of the same order as the resonant wavelength, enabling the MNPs far-field coupling, iii) a sufficiently large number of MNPs [9]. The plasmonic resonance lineshape narrowing is additionally dependent on MNP environment symmetry which must be compatible with grazing mode propagation [10]. Extensive work has been performed on these SLRs which enhance sensing sensitivity, improve emitting tunability [11,12], or conversely affect the visual appearance [13]. But, so far, only SLRs excited via free-space light have been investigated, in which the incident k-vector is located within the light cone [4,7,9,14,15]. To the best of our knowledge, systems allowing SLRs to be excited via in-phase evanescent coupling with purely guided modes have not yet been investigated. SLRs are compatible with near-field dipolar coupling between MNPs and thus with collective resonances inside 1D arrays [4,7,16–23] which can also occur with complex nanoparticle shapes or different resonance modes [24]. When such collective resonances occur in 1D chains of plasmonic nanoantennas, these cause the structure to behave like a waveguide

when the corresponding propagation vector is below the lightline. In this case, as for traditional propagating surface plasmons polaritons modes [25,26], such modes can be efficiently excited by coupling with a dielectric waveguide which generates hybrid photonic-plasmonic guided modes [27–31]. Then, depending on the grating period, the LSP chain can behave either as a waveguide or a diffraction grating acting on hybrid guided modes [32].

Here we numerically show that SLR can be additionally excited from such guided modes, in the case of spaced and contacting waveguides structures, thanks to the in-phase interaction between the back-propagating reflected LSP chain hybrid mode and the grazing diffraction mode occurring at lightline. The LSP collective resonances modify usual photonic properties in systems they interact with. SLR in such a guiding structure enables sharp spectral features and a very narrow resonance to emerge. Furthermore, we show that it can be achieved even in presence of a strong slow light regime occurring due to the interaction between the LSP chain plasmonic mode and the co and contra-propagating dielectric modes of the Si_3N_4 -waveguide, giving rise to a wide flat dispersion curve. For example, we show that these offer a new tunability of the Bragg grating reflectivity in the waveguide. Exploiting these features to control the properties of waveguiding structures is important for device compactness, tunability in photonic circuits, and applications like non-linear photonics or sensing. For these demonstrations, we numerically study the interaction between the dielectric waveguide, the LSP resonances, and the 1D periodic array diffraction modes near the lightline and near the first Brillouin zone (FBZ) border. While all these assumptions are supported by the calculations of the dispersion curve of an infinite 1D MNPs array, the related effects appear also clearly from the observation of transmittance, reflectance, and power extinction in the case of 50 MNPs chain integrated on a dielectric waveguide. The paper is organized as follows: the first part is dedicated to the description of the integrated structure, the design methodology, and the LSP 1D array mode excitation tunability, without diffraction effect (subwavelength period). SLR excitation is then evaluated in the case of a longer period plasmonic chain, i) placed at a non-zero distance from, and ii) placed in contact with the dielectric waveguide.

2. Design and LSP chain excitation

The structure under investigation, whose 3D depiction is shown in Fig. 1(a), consists of a single-mode waveguide with a Si_3N_4 core ($n_{Si_3N_4} = 2$) coupled to a periodic chain of Ag nanocylinders (the latter will be referred as the LSP chain), the whole being embedded in SiO_2 ($n_{SiO_2} = 1.457$). Figure 1(b) shows a portion of the structure viewed from above (in the $[xy]$ -plane), while a sketch of the structure observed from the side (in the $[xz]$ -plane) is shown in Fig. 1(c). The waveguide core has a thickness $T_g = 250\text{ nm}$ and a width $W_g = 300\text{ nm}$. The LSP chain is composed of 50 elliptic silver nanocylinders having radii a_x (fixed to 40 nm) and a_y , thickness $t = 40\text{ nm}$ and center to center distance (period) d . The value of a_x was set so that the distance between the chain elements was equal to or greater than 50 nm , a value which has been shown in previous experimental work to ensure high repeatability of the manufactured samples [28–31]. The bottom face of the chain nanocylinders and the top face of the waveguide core are spaced by D along the z -direction. The refractive index of silver has been modeled by fitting ellipsometric data. The thick horizontal and vertical lines, shown in Fig. 1(c), represent the location of the transmittance T (green line) and reflectance R (red line) monitors as well as two additional power monitors, σ_1 and σ_2 (yellow and magenta lines, respectively), for monitoring the out-coupled power along the z -direction. In the same figure, the dashed vertical line represents the injection position of the single-mode source. Simulations are performed by using a well-established FDTD commercial software (Lumerical Solutions). Two different types of calculation have been performed: (i) the first type consists in modeling the propagation of light through the finite structure and evaluating the transmittance and the reflectance, within the wavelength range $550\text{--}800\text{ nm}$, through T and R (see Fig. 1(c)), when the fundamental TE mode is injected in the dielectric waveguide; (ii) the

second type of simulation setup aims at identifying all the modes of the infinite periodic structure excited by randomly positioned and oriented dipoles, and at drawing such a way the structure dispersion curves (see [30] for further details on the calculation).

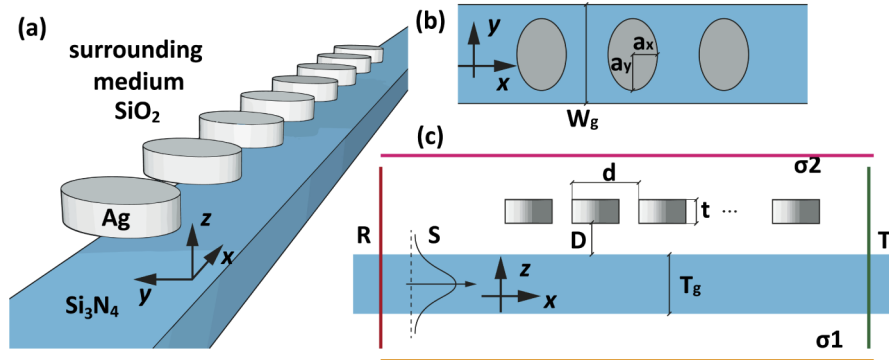


Fig. 1. (a) 3D sketch of the structure under analysis, consisting of a periodic (unidirectional) chain of elliptical silver nanocylinders placed near the core of an Si_3N_4 waveguide. The entire structure is embedded in SiO_2 . (b) A portion of the structure is depicted from above. (c) Side view of the structure. The thick green and red vertical lines represent the transmittance and reflectance monitors, respectively. The thick yellow and magenta horizontal lines represent the lower σ_1 and upper σ_2 scattering monitors, respectively. The vertical dashed line represents the injection location of the single-mode source, whose modal distribution is suggested by the bell shape.

Figure 2 shows the FDTD calculated band diagrams for only the dielectric waveguide (a), only the LSP chain (b), and the whole coupled structures when $d = 130 \text{ nm}$ and for different values of D and a_y . In Fig. 2(c-f), the observation region is bounded by the wave frequency f between 0.325 and 0.575 PHz and k_n between 0.2 and 0.5, where $k_n = d \cdot k / 2\pi$ represents the normalized wavevector. When D is large enough ($D \rightarrow \infty$), the band diagram shows the existence of two distinct, independent modes, the fundamental mode of the dielectric guide (Fig. 2(a)) and the plasmonic mode of the chain (Fig. 2(b)).

On the contrary, when D decreases, as these two modes interact thanks to their very different slopes, they interact and couple, giving rise to two distinct supermodes. For small enough D , a strongly coupled regime manifests in the opening of a gap near the intersection of their dispersion curves [30] (see the anticrossing appearing in Fig. 2(c-f)). In particular, due to the subwavelength regime in our frequency range of interest, this crossing occurs far from the FBZ edge (smaller k -vectors) and below the SiO_2 lightline (within the guided mode region). In these band diagrams, plasmonic resonance is hinted at by a blurred, weaker (brighter) curve portion indicating the spectral broadening due to high ohmic losses. In particular, the position of the LSP chain resonance is highlighted by a blue arrow marker and a thin dashed horizontal line. It is worth noting that, near the collective plasmonic resonance occurring at λ_c , the chain mode assumes a nearly horizontal slope and becomes increasingly slower as it approaches the edge of the FBZ. In the vicinity of this region, the plasmonic character of the mode is pronounced, with characteristic strong field confinement in a subwavelength volume. Conversely, far from the plasmonic resonance, the chain mode lies close to the SiO_2 lightline, where it exhibits a less plasmonic character, with much less confined fields. Finally, modes that are more localized within the dielectric waveguide core are indicated by thinner and more intense (darker) features, indicating lower or no ohmic losses. By inspecting Fig. 2, we can observe that an increase in a_y or decrease in D results in a redshift of the LSP chain resonance. The values of λ_c , as a function of a_y and D , are given in Table 1.

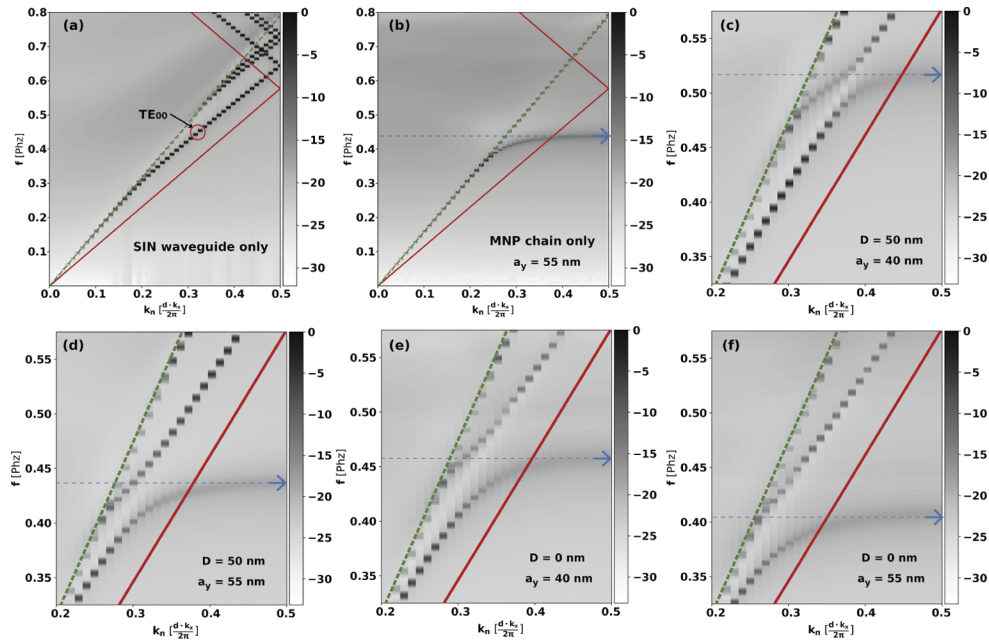


Fig. 2. FDTD calculated band diagrams for an infinitely long structure, with a subwavelength periodicity $d = 130 \text{ nm}$. Band structure (a) of only the dielectric waveguide and (b) of only the LSP chain. (c-f) Band structure of the coupled structures. (c) and (d) are calculated when $D = 50 \text{ nm}$ (spaced waveguides), while in (e) and (f) $D = 0 \text{ nm}$ (contacting waveguides). (c) and (e) are calculated when $a_y = 40 \text{ nm}$, while in (b), (d), and (f) $a_y = 55 \text{ nm}$. The continuous red line and the dashed green line represent the trace of the SiN and the SiO₂ light cones, respectively. The thin dashed blue lines, terminated on blue arrow markers, indicate the position of the LSP chain resonance λ_c . In (a) the red circle identifies the fundamental mode TE_{00} of the dielectric waveguide.

Table 1. The spectral position of the LSP chain collective plasmonic resonance as a function of a_y and D .

a_y [nm]	$D=\infty$		$D=50$ [nm]		$D=0$ [nm]	
	f [PHz]	λ [nm]	f [PHz]	λ [nm]	f [PHz]	λ [nm]
35	0.546	549	0.544	551	0.481	623
40	0.518	578	0.516	581	0.457	656
45	0.482	622	0.481	623	0.423	709
50	0.459	653	0.457	656	0.406	737
55	0.438	685	0.436	688	0.389	771

Since the losses in the dielectric waveguide core are negligible, the LSP chain excitation degree can be as well hinted at by its extinction, that is the sum of the optical power absorbed within and of that scattered/diffracted out of the structure (i.e. 1-T-R). Near the phase matching of the structure coupled modes, which occurs close to the LSP chain resonance wavelength λ_c , the transmission through the waveguide shows a dip due to maximal energy transfer from the core to the LSP chain. Figure 3 depicts the transmission spectra for a 10 elements long chain, having a period of 130 nm (no diffraction in the visible range) and $a_x = 40 \text{ nm}$, $a_y = 50 \text{ nm}$, in the case of four increasing D values. The rapid change in the wavelength corresponding to a transmittance minimum illustrates the high sensitivity of the LSP resonance to the immediate environment

(surrounding optical index, proximity of interfaces). However, for $D \geq 50 \text{ nm}$, the LSP chain resonance is no longer strongly influenced by the immediate presence of the dielectric waveguide, and the excitation efficiency decreases because of the weaker waveguides coupling. It is worth noticing that, for these values of D , the refractive index profile in the immediate vicinity of the LSP chain can be approximated as being symmetric. Conversely, the spectrum for $D = 0 \text{ nm}$ is strongly red-shifted because of the high-index waveguide core touching the MNPs, leading to a very asymmetric environment surrounding the chain. Besides, the same curve shows an irregular shape due to the occurrence of different excitation regimes of the chain [28,30]. Hereinafter, we will refer to both these configurations as the spaced ($D = 50 \text{ nm}$) and the contacting ($D = 0 \text{ nm}$) configurations.

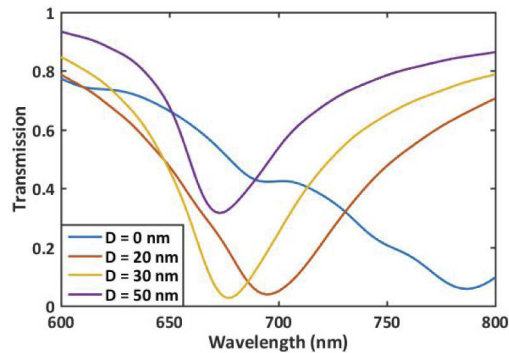


Fig. 3. Transmittances, calculated for different values of D , when a subwavelength period $d = 130 \text{ nm}$ and 10 MNPs having $a_x = 40 \text{ nm}$, $a_y = 50 \text{ nm}$, are considered.

3. SLR in spaced configuration ($D = 50 \text{ nm}$)

Figure 4(a-c) shows the transmittance, the reflectance, and the power extinction spectra calculated for the structure under investigation, in the case of a 50 period long MNPs chain having a period of 225 nm , for the spaced configuration ($D = 50 \text{ nm}$). In particular, these quantities are shown as a function of the MNPs radius a_y , when a_x is fixed at 40 nm . In accord with the results shown in Fig. 2, the coupling between the dielectric waveguide and the plasmonic chain modes is expected to be weaker with respect to the contacting configuration ($D = 0 \text{ nm}$) because of the higher separation distance D . By inspecting Fig. 4(a-c), it is possible to observe a strong dependence of the spectral features on a_y . This behavior is expected, since, as we have shown, a_y affects the spectral position of the LSP chain resonance. Conversely, a very narrow unexpected line can be clearly observed close to 726 nm (0.413 PHz) for the three maps that does not depend on a_y : it marks a strong dip or peak on transmission, reflection, and extinction spectra.

In order to fully identify these behaviors, it is essential to analyze the band diagrams of the infinite structure. Figure 5 shows a band formation scheme via hand-drawn (Fig. 5(1u-4c)) and actual band diagrams calculated via FDTD (Fig. 5(a-d)) when $D = 50 \text{ nm}$ and $d = 225 \text{ nm}$. It is worth pointing out that, in this case, the period is comparable to the minimum wavelength of interest, $\lambda/d = 550 \text{ nm}/225 \text{ nm} \approx 2.4$. Figure columns refer to different value of $a_y = 40, 45, 50$, and 55 nm . To better visualize the most important features, the figure only shows the region bounded by f between 0.325 and 0.575 PHz and k_n between 0.4 and 0.5 . The dashed green and the solid red superimposed lines stand for the silica and the Si_3N_4 waveguide core lightlines, respectively. The position of the lightlines allows us to identify the region of guided modes, which lies below the first folding of the SiO_2 lightline, labeled as F_L (indicated by a circular mark in Fig. 5(1u) and reported in Table 2) and occurring at 0.457 PHz (656 nm), and the region of

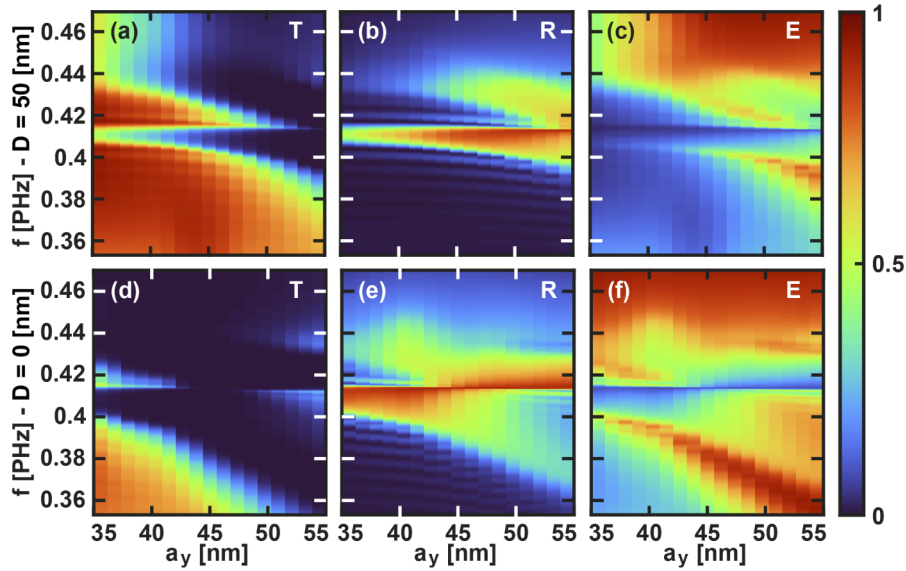


Fig. 4. (a)(d) Transmittance, (b)(e) reflectance and (c)(f) power extinction spectra, calculated for a 50 elements long chain (having $a_x = 40 \text{ nm}$ and $d = 225 \text{ nm}$) when (a-c) $D = 50 \text{ nm}$ and (d-f) $D = 0 \text{ nm}$, as a function of the radius a_y directed along y-direction of the MNPs elliptical section.

radiative modes (leaky modes), spectrally located above F_L . This is in good agreement with Figs. 4(a-c) which show an area of high transmittance, low reflectance, and moderate extinction, corresponding to the region of guided modes, and an area of high extinction, low reflectance, and weak transmittance corresponding to the region of radiative modes.

Table 2. Spectral position of points F_L , X, and F_{WG} .

	F_L	X	F_{WG}
f [PHz]	0.457	0.428	0.413
λ [nm]	656	700	726

The first and second figure rows are referred to structures taken individually (uncoupled case, see Fig. 5(1u-4u)) and to structures placed at a finite distance (coupled case, see Fig. 5(1c-4c)), respectively. The purpose of these first two figure rows is to help in identifying the different modes that can be observed in FDTD band diagrams and to explain how they interact resulting in gap formation. In the first figure row, the thick continuous magenta and cyan lines represent the ideal dispersion curves of the LSP chain and of the dielectric waveguide, respectively, when artificially folded at the FBZ edge to fit the given period $d = 225 \text{ nm}$. These folding occur at F_L for the LSP chain and at about 0.413 PHz (726 nm) for the dielectric waveguide, a point we label as F_{WG} and indicate by a circular mark in Fig. 5(1u) (its spectral position is reported in Table 2). Since the dispersion curve of the LSP chain exists only when its collective resonance exists, folding will not be observed above the plasmonic resonance maximum frequency. Additionally, Fig. 5(1u) shows that for $a_y = 40 \text{ nm}$ the crossing between the two modes occurs very close to the lightline at 0.428 PHz (700 nm), near a point denoted as X (see Fig. 5(1u), the spectral position is also reported in Table 2) and defined by the intersection of the SiO_2 lightline and the folded branch of the fundamental mode dispersion curve of the dielectric waveguide. In this case, the LSP chain resonance is located at 0.516 PHz (581 nm), i.e. significantly higher

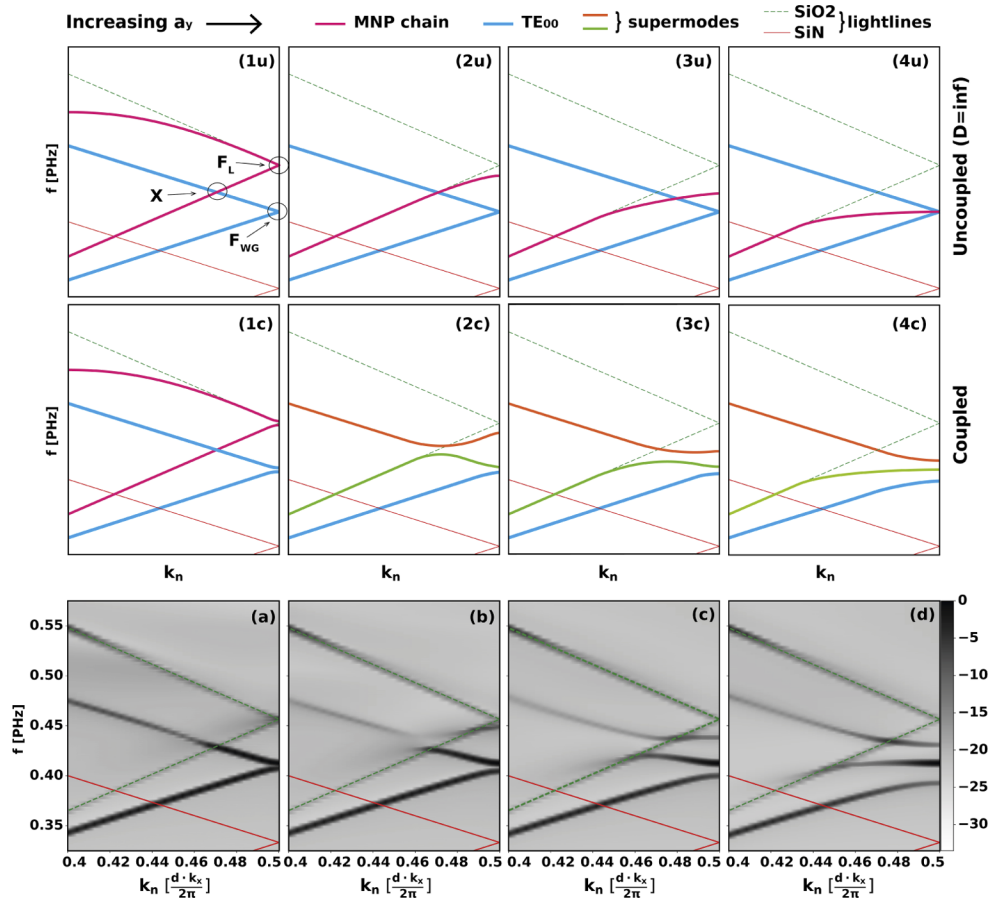


Fig. 5. (1u-4c) Hand-drawn band diagram schematics of the dispersive behavior of the (1u-4u) uncoupled (infinite D) and (1c-4c) coupled (finite D) modes of the LSP chain and dielectric waveguide. (a-d) FDTD calculated band diagrams for the spaced configuration when $D = 50$ nm and $d = 225$ nm. The continuous red line and the dashed green line represent the SiN and the SiO₂ lightlines, respectively. (a), (b), (c) and (d) correspond to $a_y = 40, 45, 50,$ and 55 nm, respectively.

than the F_L point. Moreover, near the X point, the effective index of the LSP chain mode is very close to the index of the surrounding medium (silica), revealing a very weak plasmonic character. This implies that the LSP chain mode has no way of being efficiently excited by the fundamental mode of the dielectric guide and, therefore, it does not result in a gap opening. In fact, when the structure begins to weakly couple, such as in Figs. 5(1c) and 5(a), only two edge-type small band-gaps may open at F_L and F_{WG} . Moreover, the dielectric branch weakly interacts with the plasmonic one, and crosses the lightline at X point, becoming slightly lossy. The band-gap occurring at F_{WG} results in a reflectivity peak (due to the occurrence of the Bragg grating condition for the given d) observed in Fig. 4(b) for the same value of a_y . On the contrary, near the X point and above, an increased reflectance and extinction denote the excitation of a radiative, counter-propagative mode on the LSP chain having a weak plasmonic character, as hinted by the absence of a neat extinction peak. Finally, in Fig. 5(a) the LSP chain mode, near the F_L point, manifests as a weak lossy resonance and no real gap features are visible. In contrast,

above the F_L point (for high f and low k), the plasmonic branch manifests as a very faint blurred shadow indicating conspicuous ohmic and radiation losses.

In Figs. 5(2u), 5(2c), 5(b) and Figs. 5(3u), 5(3c), 5(c), corresponding to $a_y = 45 \text{ nm}$ and 50 nm , respectively, an inner-type band-gap opens nearby the point X as the result of the counter-propagative interaction between the folded branch of the dielectric waveguide mode and the LSP chain mode. This happens because λ_c redshifts and, as a result, the intersection of the dispersion curves of the two modes occurs in a region where the plasmonic character of the LSP chain is stronger. It is worth noting that the dielectric branch "folds" toward the plasmonic branch and becomes strongly lossy (blurred), due to radiation losses as within the light cone, and to ohmic losses due to the stronger hybridization with the plasmonic mode. In Fig. 4, for the same values of a_y , we can observe the spectral signature of the two gaps, which manifest as a dip in transmittance and a peak in reflectance. We can also observe that, in Figs. 5(2u), 5(2c), and 5(b), near the inner-type gap, supermodes dispersion curves (see green and orange curves in Fig. 5(2c)) form two regions with near-zero slope. The lower one manifests in Fig. 4(c) as an extinction peak due to a counter-propagating slow light regime. The same spectral signature is observed for the lower edge of the gap near F_{WG} . Surprisingly, the upper counterpart of the gap near F_{WG} , manifests itself with a very narrow dip in extinction and peak in transmittance, both spectrally located slightly above the F_{WG} point.

Finally, in Figs. 5(4u), 5(4c), 5(d), corresponding to $a_y = 55 \text{ nm}$, the stronger redshift results in a receding of the mode crossing point from the lightline. In particular, for this specific geometrical configuration, the two-modes crossing occurs right at the point F_{WG} , resulting in three parallel branches. It is worth noticing that the central branch is now an almost spectrally flat line connecting the SiO_2 lightline to the FBZ edge. This flat branch occurring at 0.413 PHz (726 nm) is the result of hybridization between the plasmonic and dielectric waveguide modes, and it was expected to have a strongly plasmonic character, characterized by substantial losses and further enhanced by the almost-zero group velocity. However, observation of the transmittance, reflectance, and power extinction maps in Fig. 4 shows that, in the immediate vicinity of this band feature, the behavior deviates from expectations. Instead, a 2 nm -wide symmetric dip in the power extinction appears, which is matched by a symmetric peak in both the transmittance and the reflectance. We attribute this behavior to the excitation of an SLR mode.

By further increasing the value of a_y , due to the additional redshift, the crossing point moves below the first branch of the lightline. As already studied in [30], this will result in strong, co-propagative coupling.

To better visualize and explain the different mechanisms occurring near the two-modes crossing, in Fig. 6(a-c), zoomed spectra extracted from Fig. 4(a-c) are overlaid for nine discrete values of a_y . For $a_y = 45, 47.5$ and 50 nm , it is possible to identify the power extinction peaks occurring at about $704, 710$, and 716 nm , respectively, as the signature of the lower branch of the two-modes anticrossing. When a_y increases, the transmission and reflection spectra deviate from the typical profiles observed in short Bragg gratings (50 periods) into enhanced and asymmetric shapes, as long as the plasmonic resonance approaches the F_{WG} point. These asymmetrical shapes can be attributed to Fano-like resonances, due to the coupling of the narrowband SLR and the broadband plasmonic resonance which act respectively as the sharp and broad modes as extensively described and analyzed in [33]. Finally, for $a_y = 55 \text{ nm}$, Figs. 6(a-c) show an enhanced reflectance and power extinction on the whole considered spectral range except for a 2 nm -wide ($Q \approx 380$) symmetric peak or dip. We attribute this behavior to the fact that at this peculiar point, the crossing of the two modes occurs precisely at F_{WG} , which represents the boundary between the co-propagating and counter-propagating coupling regimes.

Here, an SLR is coupled to and upheld by a collective non-propagating plasmonic resonance of the LSP chain. The perfect phase matching between the co- and contra-propagative hybrid modes and the collective LSP resonance generates the flat dispersion curve of the SLR inside the

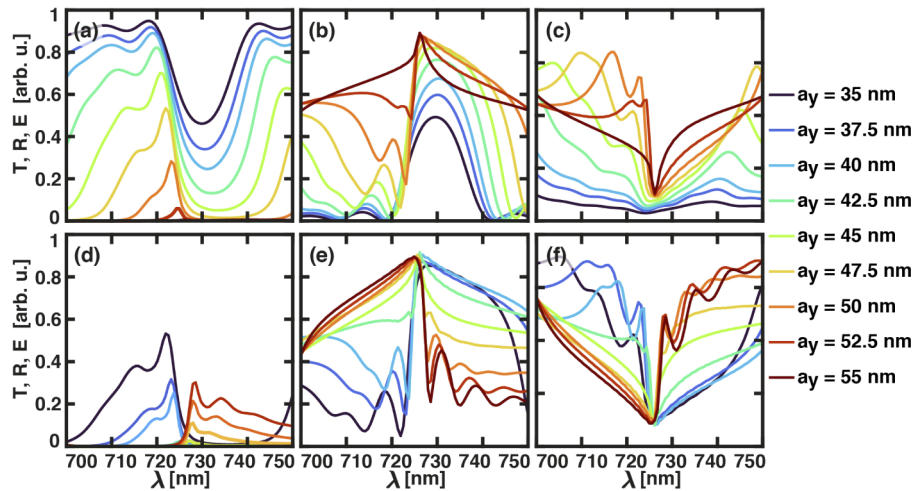


Fig. 6. (a)(d) Transmittance, (b)(e) reflectance and (c)(f) power extinction spectra of a 50 element long chain (having $a_x = 40 \text{ nm}$) when (a-c) $D = 50 \text{ nm}$ and (d-f) $D = 0 \text{ nm}$, calculated for different values of a_y .

grating gap from the FBZ border down to the lightline. Since the phase matching between the three components (propagating hybrid modes and LSP chain resonance) is a quite constraining condition, it occurs at a specific frequency and the SLR appears, as expected, at a narrow bandwidth.

These simulation results demonstrate thus the possible excitation of SLR in a 1D LSP array integrated on a dielectric waveguide, by a hybrid photonic-plasmonic mode of the coupled waveguides, in a quasi-symmetric environment. SLR is excited through a wavevector below the lightline, parallel to the array axis, and with a polarization perpendicular to it.

Besides, in addition to this SLR excitation Figs. 6(a-c) also show that in the case of moderate Bragg reflector ($a_y = 45 \text{ nm}$, maximum reflection = 0.5) the contribution of the plasmonic resonance induces significant reflection enhancement (increasing R up to 0.8, for $a_y = 55 \text{ nm}$) without modification of the central frequency. This is also an interesting property of this LSP chain to tune independently characteristics of Bragg reflectors.

4. SLR in contacting configurations ($D = 0 \text{ nm}$)

A similar study can be performed in the case of a plasmonic chain directly in contact with the dielectric waveguide ($D = 0 \text{ nm}$). In that case, a stronger coupling occurs between the dielectric waveguide and the plasmonic waveguide [28,30]. Due to the direct contact between the bottom surface of the chain MNPs and the Si_3N_4 core of the dielectric waveguide the plasmonic resonance undergoes a strong redshift. In particular, when a_y spans from 35 nm to 50 nm , the LSP chain resonance shifts from 0.481 PHz (623 nm) to 0.406 PHz (737 nm) (see Table 1). Since the period is unchanged ($d = 225 \text{ nm}$), the position of the X, F_L , and F_{WG} reference points remains unchanged. This has a direct impact on the spectral features of the structure which, as we can see from Figs. 4(d,e,f) and Figs. 6(d,e,f), occur at the same frequencies as in the spaced configuration (Figs. 4(a,b,c) and Figs. 6(a,b,c)) but for smaller values of a_y . Nevertheless, the effect of the reduction of D manifests itself in a different intensity distribution observed in these power spectra. Band diagrams in Fig. 7 also show similar characteristics as in the case $D = 50 \text{ nm}$, with stronger couplings: for $a_y = 35 \text{ nm}$, the two-modes gap begins to open at the X point and becomes wider, progressively moving away from point X, as a_y increases. The stronger two-mode coupling, which manifests with the formation of wider gaps, is due to the more efficient excitation of LSP

chain modes, which leads to an almost complete power transfer from the dielectric waveguide to the plasmonic 1D array within a very short length [28].

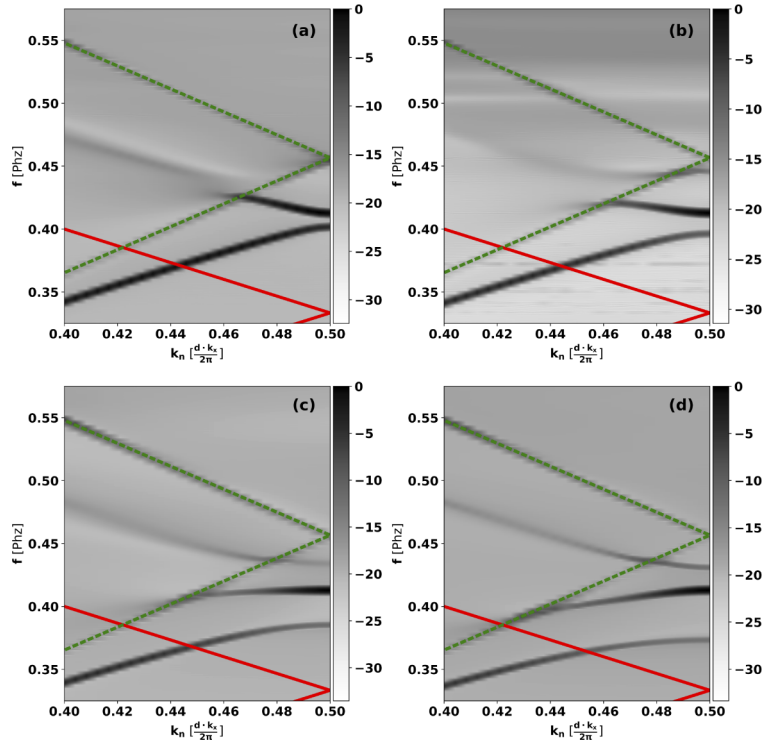


Fig. 7. FDTD calculated band diagrams for the contacting configuration, when $D = 0 \text{ nm}$ and $d = 225 \text{ nm}$. The continuous red line and the dashed green line represent the SiN and the SiO_2 lightlines, respectively.: (a), (b), (c) and (d) correspond to $a_y = 35, 40, 45,$ and 50 nm , respectively.

For $a_y = 45 \text{ nm}$, in Fig. 7(c), the two-modes crossing occurs in the vicinity of the point F_{WG} . Also in this strongly asymmetric environment, the coupling balance results in three parallel branches. The central one, occurring close to 0.413 PHz (726 nm), connects the SiO_2 lightline to the FBZ edge. Figure 4 shows that, even for $D = 0$, a 2 nm -wide symmetric dip in the power extinction appears, together with corresponding symmetrical peaks in both transmittance and reflectance, which we attribute to the excitation of the SLR mode. To further shed light on the nature of this feature, we also studied the scattering of light along the z -axis by calculating the power spectra along the two horizontal monitors indicated as σ_1 and σ_2 in Fig. 1. Figure 8(a) shows two sets of curves: (i) the transmittance (multiplied by 100), the reflectance, and the power extinction spectra, shown as solid curves; (ii) the outward power spectra through the two aforementioned horizontal monitors (multiplied by 10) and the overall power leaving the system (denoted as σ_0), shown as dashed curves. Scale factors have been added to display all different quantities on the same figure. From these spectra, we observe that at the F_{WG} point the dip in the extinction is accompanied by a dip in the curves representing the power leaving the system along the z -direction and by an increase in the power leaving the system along the direction parallel to the LSP chain. Finally, Figs. 8(b,c) show the distributions of the Poynting vector x -component and of the electric field y -component phase calculated at 0.413 PHz (726 nm). From the Poynting vector, it is possible to observe that, at this frequency, the LSP chain shows a steady-state resonance, with the energy surrounding the chain directed co-propagatively inside

the MNPs and counter-propagatively outside them. Furthermore, from the phase map, we observe that the equiphase fronts of the hybrid wave are perfectly planar and in phase with the resonance of the LSP chain, as expected for an SLR mode.

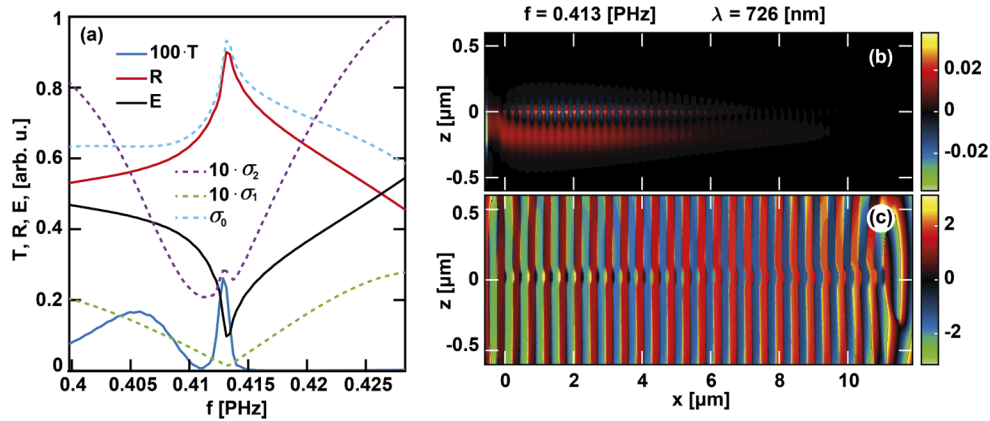


Fig. 8. (a) Transmittance T (multiplied by 100), reflectance R and power extinction E calculated for the contacting configuration when $D = 0 \text{ nm}$, $d = 225 \text{ nm}$ and $a_y = 45 \text{ nm}$ (blue, red and black solid curves, respectively); outgoing power spectra through the two horizontal monitors σ_1 and σ_2 (multiplied by 10) and the overall power leaving the system σ_0 (violet, green and cyan dashed curved, respectively). (b) Distributions of the x-component of the Poynting vector and of (c) the phase of the electric field y-component, both calculated at 0.413 PHz (726 nm).

Furthermore, since the whole hybrid modes are involved in the excitation of the SLR, the phenomenon is quite robust with respect to the spacing D between the waveguides: SLR can appear as long as the hybrid modes exist.

5. Conclusion

As shown in this paper, 1D surface lattice resonances can be excited from hybrid photonic-plasmonic guided modes, below the light line, by design parallel to the periodic LSP chain axis, in spaced or contacting waveguides configurations. In this fully waveguided structure, the grazing diffraction mode coupled to LSP chain collective resonance is excited when the photonic and plasmonic dispersion curves cross at the first Brillouin zone border, generating a wide k -band flat branch, which in turn crosses the light line. This specific phase-matched slow light results in a 2 nm -wide symmetric dip in the power extinction spectrum, which is matched by a symmetric peak in both the transmittance and the reflectance of the functionalized waveguide. Such optical response can be exploited for high-sensitivity sensors or non-linearity enhancement in case of interaction of the LSP chain with coating materials. The guiding configuration ensures the focused and efficient excitation of the involved plasmonic structures. Besides, even out of the "perfect" phase-matching leading to SLR, we have shown that the Bragg grating reflectivity can be significantly enhanced by the plasmonic resonance, without modification of its spectral position. These results open the road to new integrated photonic functions exploiting slow light or finely tuned mirror reflectivity based on localized surface plasmon resonances.

Funding. Regione Puglia (Research for Innovation (REFIN)).

Acknowledgments. GM is supported by a grant from Regione Puglia "Research for Innovation" (REFIN). REFIN is an intervention co-financed by the European Union under the POR Puglia 2014-2020, Priority Axis OT X "Investing in education, training and professional training for skills and lifelong learning - Action 10.4 - DGR 1991/2018 - Notice 2/FSE/2020 n. 57 of 13/05/2019 (BURP n. 52 of 16/06/2019)

Disclosures. The authors declare no conflicts of interest.

Data availability. Data underlying the results presented in this paper are not publicly available at this time but may be obtained from the authors upon reasonable request.

References

1. K. L. Kelly, E. Coronado, L. L. Zhao, and G. C. Schatz, "The optical properties of metal nanoparticles: the influence of size, shape, and dielectric environment," *J. Phys. Chem. B* **107**(3), 668–677 (2003).
2. A. Kristensen, J. K. W. Yang, S. I. Bozhevolnyi, S. Link, P. Nordlander, and N. J. M. N. A. Halas, "Plasmonic colour generation," *Nat. Rev. Mat.* **2**(1), 16088 (2017).
3. S. Zou, N. Janel, and G. C. Schatz, "Silver nanoparticle array structures that produce remarkably narrow plasmon lineshapes," *J. Chem. Phys.* **120**(23), 10871–10875 (2004).
4. V. G. Kravets, F. Schedin, and A. N. Grigorenko, "Extremely narrow plasmon resonances based on diffraction coupling of localized plasmons in arrays of metallic nanoparticles," *Phys. Rev. Lett.* **101**(8), 087403 (2008).
5. Y. Chu, E. Schonbrun, T. Yang, and K. B. Crozier, "Experimental observation of narrow surface plasmon resonances in gold nanoparticle arrays," *Appl. Phys. Lett.* **93**(18), 181108 (2008).
6. B. Augu e and W. L. Barnes, "Collective resonances in gold nanoparticle arrays," *Phys. Rev. Lett.* **101**(14), 143902 (2008).
7. S. Zou and G. C. Schatz, "Narrow plasmonic/photonic extinction and scattering line shapes for one and two dimensional silver nanoparticle arrays," *J. Chem. Phys.* **121**(24), 12606 (2004).
8. V. A. Markel, "Divergence of dipole sums and the nature of non-lorentzian exponentially narrow resonances in one-dimensional periodic arrays of nanospheres," *J. Phys. B: At., Mol. Opt. Phys.* **38**(7), L115–L121 (2005).
9. S. Zou and G. C. Schatz, "Theoretical studies of plasmon resonances in one-dimensional nanoparticle chains: narrow lineshapes with tunable widths," *Nanotechnology* **17**(11), 2813–2820 (2006).
10. V. G. Kravets, A. V. Kabashin, W. L. Barnes, and A. N. Grigorenko, "Plasmonic surface lattice resonances: a review of properties and applications," *Chem. Rev.* **118**(12), 5912–5951 (2018).
11. A. V. Kabashin, S. Patskovsky, and A. N. Grigorenko, "Phase and amplitude sensitivities in surface plasmon resonance bio and chemical sensing," *Opt. Express* **17**(23), 21191–21204 (2009).
12. T. Teperik and A. Degiron, "Superradiant optical emitters coupled to an array of nanosize metallic antennas," *Phys. Rev. Lett.* **108**(14), 147401 (2012).
13. H. Bertin, Y. Br l e, G. Magno, T. Lopez, P. Gogol, L. Pradere, B. Gralak, D. Barat, G. Dem sy, and B. Dagens, "Correlated disordered plasmonic nanostructures arrays for augmented reality," *ACS Photonics* **5**(7), 2661–2668 (2018).
14. R. Guo, T. K. Hakala, and P. T rm , "Geometry dependence of surface lattice resonances in plasmonic nanoparticle arrays," *Phys. Rev. B: Condens. Matter Mater. Phys.* **95**(15), 155423 (2017).
15. Y. Hua, A. K. Fumani, and T. W. Odom, "Tunable lattice plasmon resonances in 1D nanogratings," *ACS Photonics* **6**(2), 322–326 (2019).
16. M. Quinten, A. Laitner, J. R. Krenn, and F. R. Aussenegg, "Electromagnetic energy transport via linear chains of silver nanoparticles," *Opt. Lett.* **23**(17), 1331–1333 (1998).
17. M. L. Brongersma, J. W. Hartman, and H. A. Atwater, "Electromagnetic energy transfer and switching in nanoparticle chain arrays below the diffraction limit," *Phys. Rev. B: Condens. Matter Mater. Phys.* **62**(24), R16356 (2000).
18. S. A. Maier, M. L. Brongersma, and H. A. Atwater, "Electromagnetic energy transport along arrays of closely spaced metal rods as an analogue to plasmonic devices," *Appl. Phys. Lett.* **78**(1), 16–18 (2001).
19. W. H. Weber and G. W. Ford, "Propagation of optical excitations by dipolar interactions in metal nanoparticle chains," *Phys. Rev. B* **70**(12), 125429 (2004).
20. A. F. Koenderink and A. Polman, "Complex response and polariton-like dispersion splitting in periodic metal nanoparticle chains," *Phys. Rev. B* **74**(3), 033402 (2006).
21. A. Al  and N. Engheta, "Theory of linear chains of metamaterial/plasmonic particles as subdiffraction optical nanotransmission lines," *Phys. Rev. B* **74**(20), 205436 (2006).
22. S. Zou and G. C. Schatz, "Metal nanoparticle array waveguides: proposed structures for subwavelength devices," *Phys. Rev. B* **74**(12), 125111 (2006).
23. K. B. Crozier, E. Togan, E. Simsek, and T. Yang, "Experimental measurement of the dispersion relations of the surface plasmon modes of metal nanoparticle chains," *Opt. Express* **15**(26), 17482–17493 (2007).
24. A. M. Pikalov, A. V. Dorofeenko, and Y. E. Lozovik, "Dispersion relations for plasmons in complex-shaped nanoparticle chains," *Phys. Rev. B* **98**(8), 085134 (2018).
25. J.-C. Weeber, Y. Lacroute, and A. Dereux, "Optical near-field distributions of surface plasmon waveguide modes," *Phys. Rev. B* **68**(11), 115401 (2003).
26. G. Magno, M. Grande, V. Petruzzelli, and A. D'Orazio, "Numerical analysis of the coupling mechanism in long-range plasmonic couplers at 1.55 μm ," *Opt. Lett.* **38**(1), 46–48 (2013).
27. C. Delacour, S. Blaize, P. Grosse, J. M. Fedeli, A. Bruyant, R. Salas-Montiel, G. Lerondel, and A. Chelnokov, "Efficient directional coupling between silicon and copper plasmonic nanoslot waveguides: toward Metal-Oxide-Silicon nanophotonics," *Nano Lett.* **10**(8), 2922–2926 (2010).

28. M. Février, P. Gogol, A. Aassime, R. Mégy, C. Delacour, A. Chelnokov, A. Apuzzo, S. Blaize, J.-M. Lourtioz, and B. Dagens, "Giant coupling effect between metal nanoparticle chain and optical waveguide," *Nano Lett.* **12**(2), 1032–1037 (2012).
29. M. Février, P. Gogol, G. Barbillon, A. Aassime, R. Mégy, B. Bartenlian, J.-M. Lourtioz, and B. Dagens, "Integration of short gold nanoparticles chain on SOI waveguide toward compact integrated bio-sensors," *Opt. Express* **20**(16), 17402–17409 (2012).
30. G. Magno, M. Fevrier, P. Gogol, A. Aassime, A. Bondi, R. Mégy, and B. Dagens, "Strong coupling and vortices assisted slow light in plasmonic chain-SOI waveguide systems," *Sci. Rep.* **7**(1), 7228 (2017).
31. B. Dagens, M. Fevrier, P. Gogol, S. Blaize, A. Apuzzo, G. Magno, R. Megy, and G. Lerondel, "Direct observation of optical field phase carving in the vicinity of plasmonic metasurfaces," *Nano Lett.* **16**(7), 4014–4018 (2016).
32. M. Février, P. Gogol, J.-M. Lourtioz, and B. Dagens, "Metallic nanoparticle chains on dielectric waveguides: coupled and uncoupled situations compared," *Opt. Express* **21**(21), 24504–24513 (2013).
33. V. Giannini, Y. Francescato, H. Amrania, C. C. Phillips, and S. A. Maier, "Fano resonances in nanoscale plasmonic systems: a parameter-free modeling approach," *Nano Lett.* **11**(7), 2835–2840 (2011).